

SUPPLEMENTAL MATERIAL

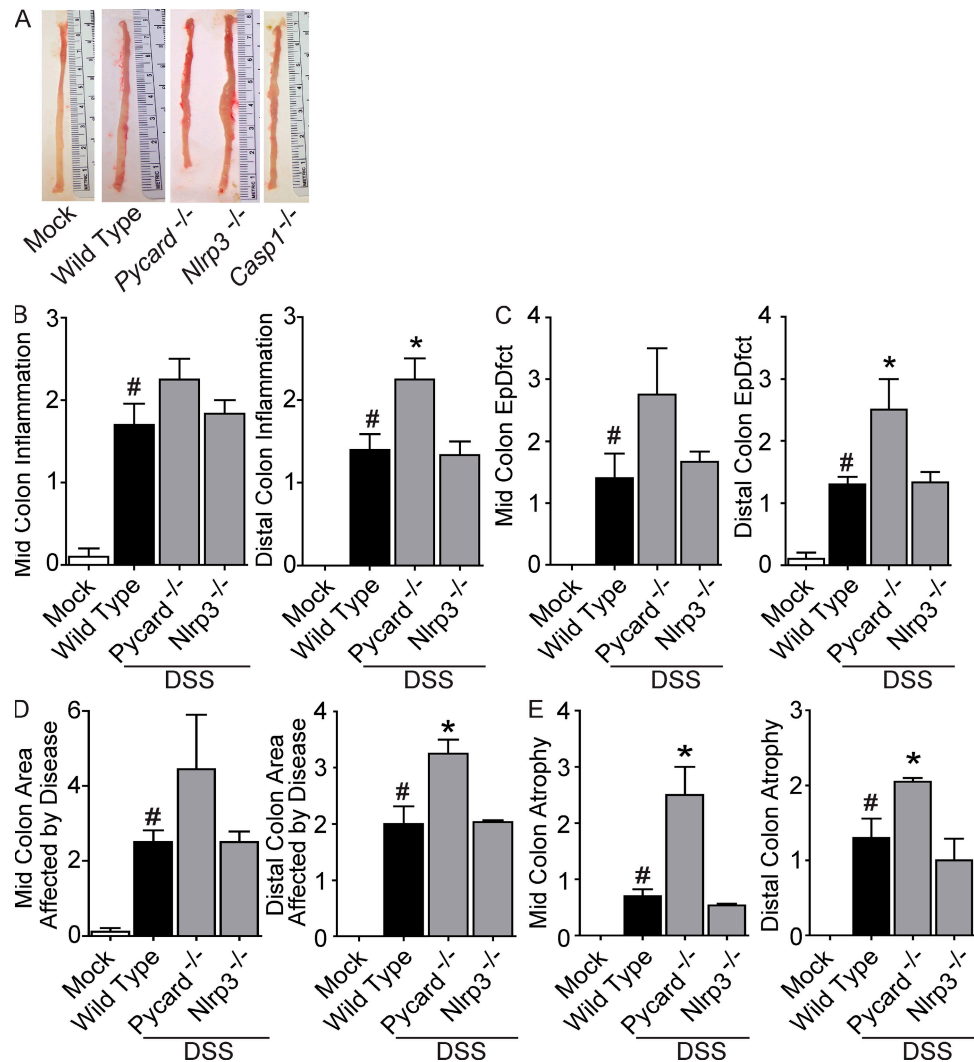
Allen et al., <http://www.jem.org/cgi/content/full/jem.20100050/DC1>

Figure S1. *Pycard^{-/-}* mice demonstrate increased mid and distal colon histopathology in the recurring ulcerative colitis model. (A) Colons harvested from *Pycard^{-/-}* and *Casp1^{-/-}* mice were truncated compared with those harvested from similarly treated WT and *Nlrp3^{-/-}* mice. No gross morphological differences were observed between colons harvested from mock-treated, WT, *Pycard^{-/-}*, *Nlrp3^{-/-}*, and *Casp1^{-/-}* mice. WT mock, $n = 3$; WT, $n = 3$; *Pycard^{-/-}*, $n = 3$; *Nlrp3^{-/-}*, $n = 5$. (B-E) Significant increases in inflammation (B), epithelial cell defects (C), the area involved with pathology (D), and increased crypt atrophy were observed in the *Pycard^{-/-}* animals (E). The symbol # indicates $P < 0.05$ between the mock and DSS-treated WT; * indicates $P < 0.05$ between the *Pycard^{-/-}* mice and WT. WT mock, $n = 5$; WT, $n = 5$; *Pycard^{-/-}*, $n = 3$; *Nlrp3^{-/-}*, $n = 3$.

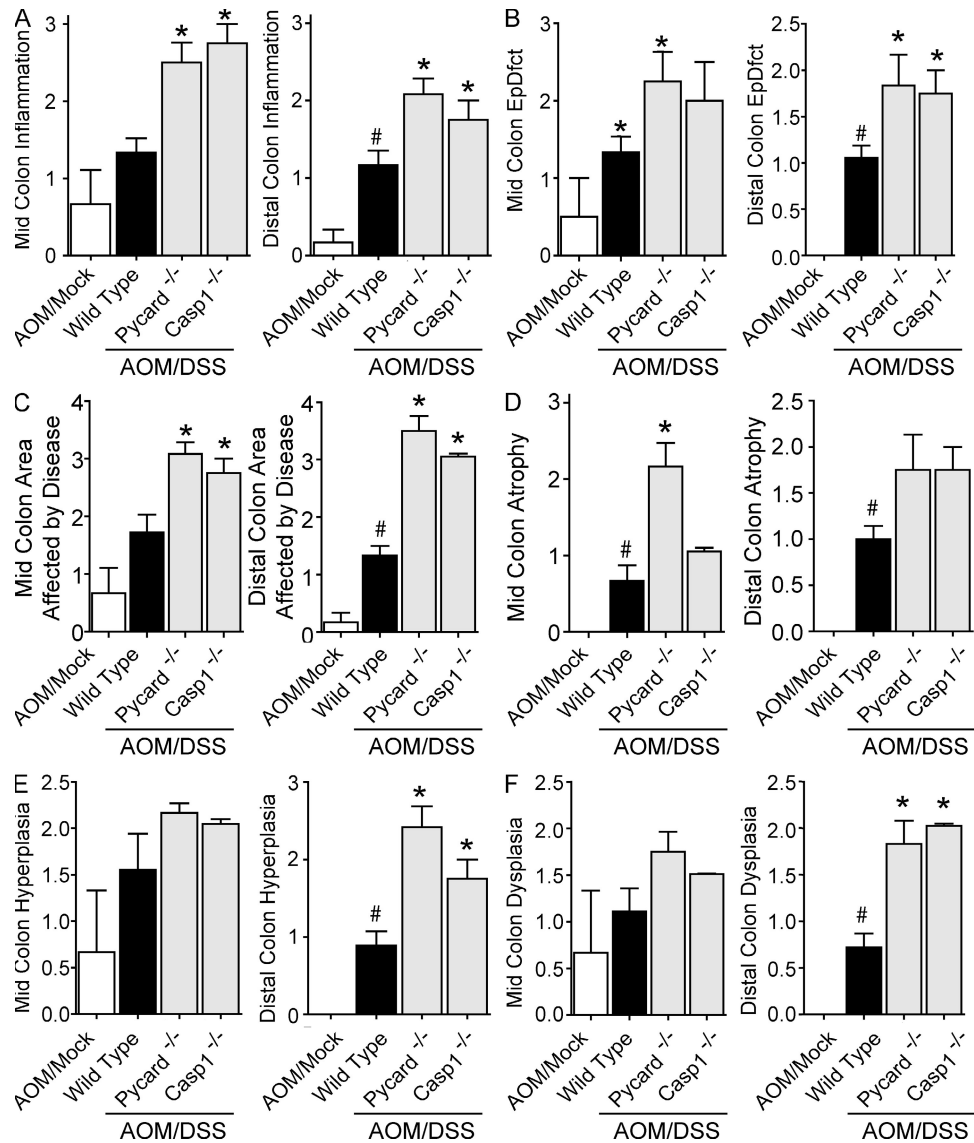


Figure S2. *Casp1^{-/-}* and *Pycard^{-/-}* mice demonstrate increased mid and distal colon histopathology in the CAC model. (A–C) Significant increases in (A) inflammation, (B) epithelial cell defects, and (C) the area involved with pathology were observed in the *Casp1^{-/-}* and *Pycard^{-/-}* mice. * and # indicates $P < 0.05$; WT AOM, $n = 3$; WT, $n = 9$; *Pycard^{-/-}*, $n = 6$; *Casp1^{-/-}*, $n = 3$. (D) A significant increase in crypt atrophy was observed in the mid colon of *Pycard^{-/-}* mice, while increased distal crypt atrophy was observed in both *Pycard^{-/-}* and *Casp1^{-/-}* mice. * and # indicates $P < 0.05$; WT AOM, $n = 3$; WT, $n = 9$; *Pycard^{-/-}*, $n = 6$; *Casp1^{-/-}*, $n = 3$. (E and F) Significant increases in distal colon hyperplasia (E) and dysplasia (F) were detected in *Pycard^{-/-}* and *Casp1^{-/-}* mice. The symbol # indicates $P < 0.05$ between the AOM/mock- and AOM/DSS-treated WT; * indicates $P < 0.05$ between the gene-deficient strains and WT. WT AOM, $n = 3$; WT, $n = 9$; *Pycard^{-/-}*, $n = 6$; *Casp1^{-/-}*, $n = 3$.

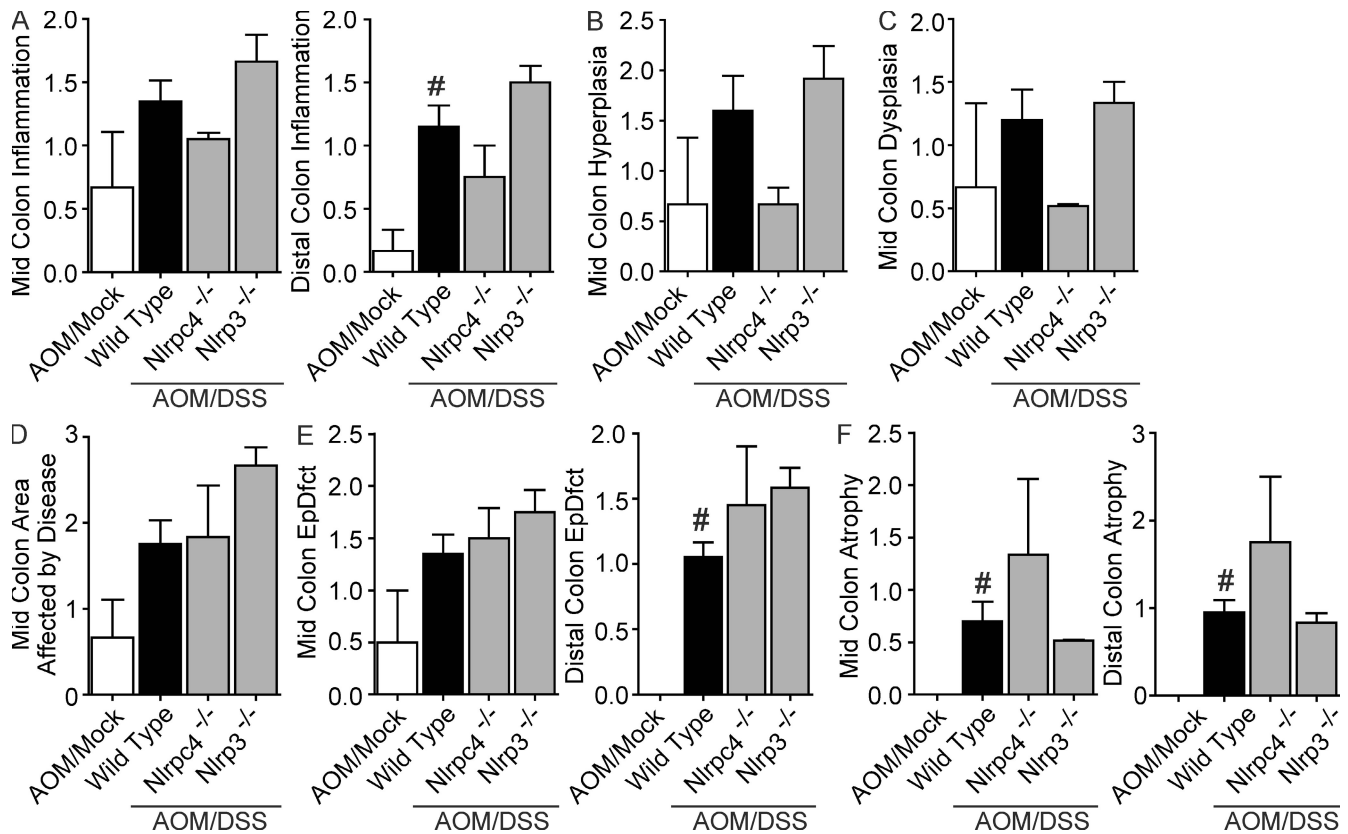


Figure S3. Increased gastrointestinal disease was localized to the distal colon in the *Nlrp3*^{-/-} mice. Inflammation (A), midcolon hyperplasia (B), mid-colon dysplasia (C), area involved in mid-colon disease (D), mid and distal colon epithelial defects (E), and mid and distal colon atrophy (F) were not significantly different between AOM/DSS-challenged mice. The symbol # indicates P < 0.05 between the AOM/mock-and AOM/DSS-treated WT; WT AOM, n = 3; WT, n = 10; *Nlrc4*^{-/-}, n = 3; *Nlrp3*^{-/-}, n = 6.

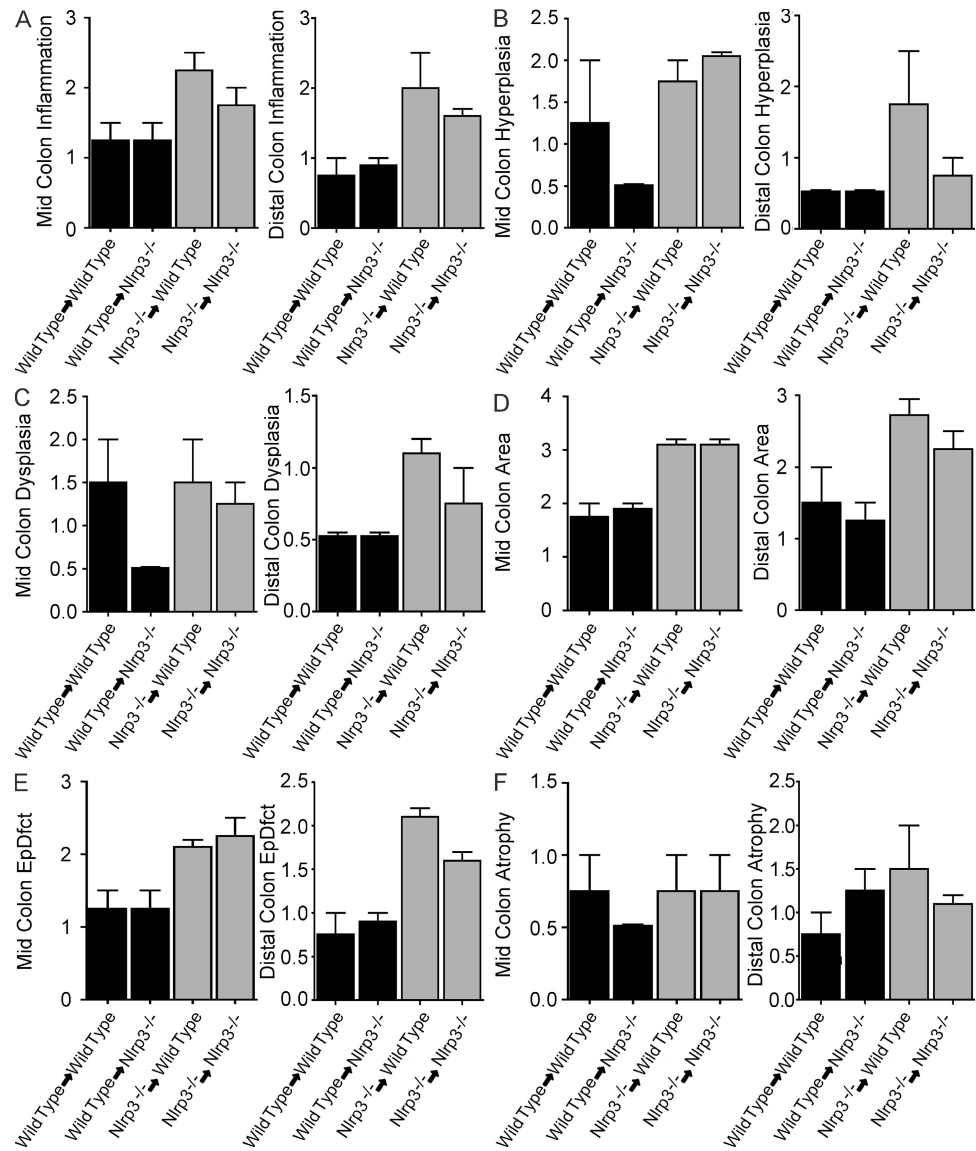


Figure S4. Increased histopathology in mice receiving *Nlrp3*^{-/-} bone marrow. (A-F) Recipients of *Nlrp3*^{-/-} bone marrow demonstrate trending increases in distal colon inflammation (A), hyperplasia (B), dysplasia (C), and area involved with disease (D). Midcolon (A) inflammation, hyperplasia (B), dysplasia (C), area involved in disease and mid and distal (D), epithelial defects (E), and crypt atrophy (F) were not significantly increased between experimental groups. WT-*Nlrp3*^{-/-}, n = 7; *Nlrp3*^{-/-}-WT, n = 7; WT-WT, n = 3; *Nlrp3*^{-/-}-*Nlrp3*^{-/-}, n = 3.